UNIVERSITY OF OKLAHOMA

GRADUATE COLLEGE

NEW INSIGHTS INTO *TENONTOSAURUS TILLETTI* (DINOSAURIA: ORNITHOPODA) FROM AN EXCEPTIONALLY PRESERVED SPECIMEN

A THESIS

SUBMITTED TO THE GRADUATE FACULTY

in partial fulfillment of the requirements for the

Degree of

MASTER OF SCIENCE

By

TYLER CRAIG HUNT
Norman, Oklahoma
2018

NEW INSIGHTS INTO *TENONTOSAURUS TILLETTI* (DINOSAURIA: ORNITHOPODA) FROM AN EXCEPTIONALLY PRESERVED SPECIMEN

A THESIS APPROVED FOR THE
DEPARTMENT OF BIOLOGY

BY

_____
Dr. Rich Cifelli, Chair

_____
Dr. Stephen Westrop

_____
Dr. Cameron Siler

_____
Dr. Nicholas Czaplewski

I dedicate this thesis to my family, for cultivating my love of the natural world and for supporting me in every possible way as I strive to achieve my childhood dream. Also, to Todd Johnson for taking me on my first fossil hunt, while my fossil collection has grown over the years, the ammonite I found on that first trip still holds a place of honor as my first major find.

Acknowledgements

First and foremost, I would like to thank the members of my committee, Rich, Steve, Nick, and Cam whose mentorship extended years prior to them joining my committee, I truly would not be here today without your guidance. To my colleagues, Joe Frederickson and Josh Cohen thank you for bringing me into the fold and teaching me how to be a productive, collaborative, scientist and for pushing me to do more than I thought I was capable of. Special thanks to Kyle Davies for being a great office mate, suffering my constant questions, and for suggesting the initial topic of my thesis. To Joe Peterson, for being a sounding board to all my pathology related questions and ideas and reviewing multiple drafts of my second chapter. To Charles Baker, for providing guidance on all things in college, life, and paleontology. Thanks to all the faculty and staff of the Department of Biology and Sam Noble Oklahoma Museum of Natural History.

I would like to sincerely thank Jeff Berry for sharing his expertise concerning Computed Tomography (CT) and the University of Oklahoma Health Sciences Center for generously providing use of their CT scanner.

Table of Content

List of Figures

Abstract

Tenontosaurus tilletti Ostrom, 1970 is one of the most completely known Early Cretaceous (Aptian-Albian) dinosaurs, represented by more than thirty partial skeletons. Even so, some questions remain about the morphology of this species, particularly concerning the rarely preserved manual elements. Herein, I present new observations from an exceptionally well-preserved subadult specimen from the Antlers Formation of southeastern Oklahoma. Oklahoma Museum of Natural History (OMNH) specimen number 58340 preserves nearly every bone in articulation including the rarely preserved distalmost phalanges. The preservation of these manual elements reveals a phalangeal formula count of 2-3-3-2-2. With the complete hand morphology now known, only digits I and II are shown to terminate with an arched claw-like ungual, a new autapomorphy of the species. In contrast, digits III, IV, and V are terminated by small sesamoid-like phalanges, which were mistakenly interpreted as distal carpal elements. Moreover, the unique preservation of this specimen makes possible inferences about the soft tissue structure of the wrist, providing insights into the function of the carpus.

In addition to the complete manus, OMNH 58340 has five trauma and infection related skeletal pathologies. The manual phalanx I-1 and left dorsal rib 10 are fractured with signs of extensive callus formation in the later stages of healing, interpreted to be contemporaneous injuries. In addition to traumatic fractures, both elements have a morphology consistent with post-traumatic osteomyelitis. Left dorsal rib 7 and right dorsal rib 10 exhibit impacted fractures that are compressed 26 mm and 24 mm, respectively. Both lack callus formation and possess a fracture morphology consistent

with pliable living bone, suggesting these fractures occurred around the time of death. Computed tomography (CT) visualizations reveal the presence of a large internal abscess in pathological metacarpal IV of OMNH 58340, with a morphology consistent with a subacute type of hematogenous osteomyelitis, termed a Brodie abscess. This is only the second report of an injury of this type in non-avian dinosaurs and the first in Ornithopoda. Based on the location and two distinct phases of healing present, I hypothesize that this individual experienced a minimum of two traumatic events (e.g., from a fall) with the injuries of the former developing chronic osseous infections.

The Revised Manus Morphology of *Tenontosaurus tilletti* (Dinosauria: Ornithopoda)

Introduction

The manus of ornithopods is consistently one of the most enigmatic, incompletely represented parts of the skeleton. Often descriptions of new genera do not include descriptions of manual elements or are described on the basis of incomplete disarticulated manus elements (Galton, 1974; Ostrom, 1970; Sereno, 1991), even among relatively well-represented taxa. This is certainly the case for *Tenontosaurus tilletti*, a medium-sized iguanodontian first described by Ostrom (1970) from the Early Cretaceous Cloverly Formation of Montana. At the time of Ostrom's (1970) work, 26 partial or nearly complete skeletons were known, of which only four examples of preserved manus were described—OMNH 10321 (formerly OU 11), BB-1, AMNH 3031 and YPM 5459 (institutional abbreviation are defined below). Unsurprisingly, the lack of articulated manus material led to confusion about the placement of some elements. In a redescription of the postcranial skeleton of *T. tilletti*, Forster (1990) noted that Ostrom had erroneously placed phalanx V-1 as the distal phalanx of digit IV and the radiale was placed as the terminal phalanx of digit V. Based on these corrections it was inferred that the phalangeal formula of *T. tilletti* is 2-3-3-1?-1? rather than the 2-3-3-2-2 as originally suggested by Ostrom (1970). Until now, this arrangement has largely gone unchallenged (Norman, 2004). The discovery of new specimens of *T. tilletti* with articulated manus from the Aptian-Albian Antlers Formation of southeastern Oklahoma indicates the need for further revision of the manus morphology.

The Antlers Formation has produced 16 partial or nearly complete skeletons of *T. tilletti* of multiple ontogenetic classes (Werning, 2012). One specimen of note, OMNH 58340, is a nearly complete, articulated, subadult *T. tilletti* skeleton with multiple elements retaining three-dimensional articulation such as the skull, pelvis, right foot, and left manus (Werning, 2012). This specimen includes rarely preserved elements such as the hyoids, atlantal ribs, and distal-most phalanges; the skeleton lacks only the middle section of the tail due to weathering prior to collection. The articulation of this individual was preserved during preparation so that all elements remain in their in situ articulation, leaving no doubts as to the positioning of the elements. Here, I revise the manus morphology of *T. tilletti* based on OMNH 58340 and two other intact manus (OMNH 62990, 63525) from the Antlers Formation. Furthermore, I make comparisons with ornithopods having well-known manus morphologies, including, *Iguanodon bernissartensis* (Boulenger, 1881), *Camptosaurus dispar* (Marsh, 1885), and *Hypsilophodon foxii* (Huxley, 1869), to make inferences about the functionality of the manus.

Institutional Abbreviations: AMNH, American Museum of Natural History, New York City, New York; BB, Buffalo Bill Center of the West, Cody, Wyoming; MOR, Museum of the Rockies, Montana State University, Montana; OMNH, Sam Noble Museum of Natural History, Norman, Oklahoma; YPM, Yale Peabody Museum of Natural History, New Haven, Connecticut

Materials & Methods

The following description is based on three nearly complete articulated manus: the left manus of OMNH 58340, the left manus of OMNH 62990, and the right manus of OMNH 63525. During preparation, the articulation among individual bones was retained by making plaster jackets that hold the bones—now free from matrix—in their original *in situ* positions (Fig. 1). All specimens were placed in their respective maturity class based on a histological study performed by Werning (2012). OMNH 58340 and OMNH 63525 are both subadult individuals, although OMNH 63525 is approximately 25% smaller than OMNH 58340. Of the three specimens, OMNH 58340 is the most complete, missing only phalanx V-2. OMNH 63525 includes the intermedium and ulnare in the carpus, preserves all five metacarpals, and is missing phalanges: I-1, I-2, III-2, III-3, and IV-2; however, this is the only manus to preserve the distal most phalanx on digit V, V-2. OMNH 62990 is from an adult specimen and preserves all elements of the manus except the distal most phalanges: III-3, IV-2, and V-2.

Geologic Context

The Antlers Formation outcrops in Oklahoma as an E-W trending band 8 to 20 miles in width and approximately 210 miles long, spanning the southeastern margin of the state, from the Arkansas border to Lake Texoma in the west, where it dips southward into Texas (Fig. 2) (Manley, 1965). It is composed of fluvial, deltaic, and strand plain sandstones deposited on the northern and western margins of the East Texas Embayment (Hobday et al., 1981). The Antlers Formation is the northern and western lateral equivalent to the Trinity Group of Texas. The Trinity Group is composed of three units: the Twin Mountains, Glen Rose, and Paluxy formations, in ascending order.

The middle unit, the Glen Rose Formation, is a transgressive shallow marine limestone that pinches out to the north and west. In the absence of the Glen Rose Formation, the terrigenous Twin Mountains and Paluxy formations are indistinguishable and therefore grouped together as the Antlers formation (Hobday et al., 1981). The age of the Antlers Formation is extrapolated from the biostratigraphic dating of invertebrates from the Trinity Group and overlying formations. While not constrained at the base, the Twin Mountains Formation is assumed to be no older than the Barremian-Aptian boundary; the beginning of the Albian is located at the base of the Glen Rose Formation, and the Paluxy Formation is constrained from above as early middle Aptian by the occurrence of the ammonite *Metengonoceras* in the Goodland Formation (Jacobs and Winkler, 1998). Therefore, as the Trinity Group's lateral equivalent, the Antlers Formation is Aptian-Albian in age.

Specimen OMNH 58340, was collected from the Antlers Formation of southeastern Atoka County, Oklahoma, at OMNH locality V821 (Fig. 2). V821 is located 1 km northeast of the better known OMNH locality, V706, that produced numerous microfossils, a partially articulated *Deinonychus antirrhopus* (Ostrom, 1969) and multiple associated *Tenontosaurus tilletti* remains, including OMNH 62990 and OMNH 63525 (Brinkman et al., 1998; Cifelli et al., 1997; Thomas, 2015). In addition to OMNH 58340, the sauropod *Sauroposeidan proteles* (Wedel et al., 2000) was found at V821 in sediments 3-5 m lower, stratigraphically. Rennison (1996) estimated the stratigraphic level of V706 to be 87 m above the base of the formation, with a total estimated thickness of 150 m, placing V706 in the upper-middle section of the formation. Therefore, the adjacent locality V821 is likely at a similar stratigraphic level.

The lithology of the Antlers is variable; locally, it is composed of laterally discontinuous bands of fine to coarse grained, moderately sorted, argillaceous to locally carbonate-cemented, ferruginous sandstones with interspersed lenses of sandy clays, typical of the Antlers Formation but lacking the poorly sorted gravel-conglomerate lenses reported in other parts of the formation (Manley, 1965). OMNH 58340 is complete, with only the mid-section of the tail missing due to weathering. Additionally, the remarkable completeness is matched by the 3D preservation and retainment of articulation in many of its elements including the left manus, right pes, pelvic girdle, and skull (see Thomas, 2015 for description of cranial elements). The preservation of rare elements and exceptional articulation suggests that this specimen was minimally transported and buried quickly with significant portions of flesh preserved. The preservation and preparation of this specimen provides a unique opportunity to make estimates of cartilage thickness from the preserved interosseous spacing.

Manus Description

OMNH 58340

While multiple other articulated manus of *Tenontosaurus tilletti* exist (i.e., OMNH 62990, 63525), the left manus of OMNH 58340 preserves all elements (except phalanx V-II) in articulation with minimal taphonomic distortion. As exposed in its plaster support holder, the hand is seen in palmar view, with digits I and II slightly flexed presumably in rigor mortis (Fig. 1), a condition typically seen in the articulated pes of this species. Digits IV and V are laterally divergent from the closely associated digits II and III. Digit V is so laterally divergent that it is closely associated with the lateral margin of the ulnare. Unlike the condition seen in other, presumably more derived

iguanodontians, the carpals and metacarpals of OMNH 58340 do not articulate, varying in their amount of separation from 7 to 30 mm. Based on the articulation and orientation of the metacarpals and phalangeal elements, the three-dimensional relationships as preserved are presumed to reflect their original anatomy and not produced by taphonomic distortion. Hereafter, the term "articulate" will be used to describe the adjacent faces of the metacarpals and carpals even though, in life, these elements were separated by considerable soft tissue and did not, in fact, articulate sensu strico.

Carpus

The carpal elements of OMNH 58340 are composed of three slightly interlocking carpals, the ulnare, the intermedium, and the radiale (Fig. 3A, B). The radiale is roughly hourglass shaped (i.e., the proximal and distal margins are flared relative to the midline). The distal surface is wide, ovate, and rugose with a small medial projection that tapers to a rounded point. The proximal surface is rugose and rounded transversely. The palmar surface is rugose and flat while the other sides are slightly convex.

The intermedium, the smallest of the three carpals, is rectangular and has flat proximal and distal surfaces. The dorsal surface is smooth and concave transversely. The palmar side is tightly concave proximo-distally. The medial side that articulates with the radiale is convex and the side that articulates with the ulnare is slightly convex, forming an integrated carpal complex.

The largest and most lateral element of the carpus is the ulnare. The dorsal face of the ulnare is smooth, transversely concave, and roughly parallelogram shaped in outline. The margins taper to form a smaller parallelogram on the palmar surface. The medial

and proximal margins are concave, forming a waist around the medial and proximal borders. The distal and lateral faces are flat and square in outline with a rounded border between them, presumably forming a buttress for articulation with the laterally oriented digits IV and V. The orientations of the intermedium and ulnare shown by Forster (1990:fig. 13) are now known to be incorrect. The smooth surface on the intermedium described by Forster (1990) as proximal is instead the dorsal surface. The corrected orientations for the ulnare and intermedium provided by Forster (1990:fig. 13) are: A) dorsal, B) proximal, C) palmar. Additionally, the manus of OMNH 58340, OMNH 62990, OMNH 63525 do not preserve distal carpal ossifications as previously suggested for *T. tilletti* (Dodson, 1980; Forster, 1990).

Forster (1990) reported that BB 1 and AMNH 3014 have a single distal carpal ossification, that YPM 5459 has two distal carpal ossifications, and that in other well-preserved specimens these ossifications are absent. In OMNH 58340 these ossifications are also absent in the carpal region and they are absent in the larger (OMNH 62990) and smaller (OMNH 63525) articulated manus, indicating that they do not ossify through ontogeny. OMNH 58340 and OMNH 63525 do, however, preserve distal phalangeal elements that are small, ovoid, sesamoid-like bones, which if disarticulated, could be confused with distal carpal ossifications. Therefore, *T. tilletti* has only three ossified carpal elements, the radiale, intermedium, and ulnare with no distal carpal ossifications; rather, the ossifications earlier termed "distal carpal elements" are the rarely-preserved, distal-most phalanges. The geologically older species, *Tenontosaurus dossi* (Winkler et al., 1997) may have had similar distal phalanges. Winkler et al. (1997, p. 340) described a "small round distal carpal" present between the intermedium and ulnare in a partially

articulated forelimb (FWMSH 93B2); however, confirmation from a more complete specimen is needed.

Metacarpals and Digits

The articulated manus of OMNH 58340 indicates that digits IV and V are closely associated and diverge laterally, and that digits I, II, III are closely associated with a pronounced medial curvature, forming a wide, manus vaguely resembling a baseball mitt, with a phalangeal formula of 2-3-3-2-2 (based on OMNH 58340, OMNH 63525, OMNH 62990). Metacarpal I is dorsoventrally compressed with a triangular proximal condyle and a sub-rectangular distal condyle. Phalanx I-1 has a short and wide diaphysis, with a well-developed sagittal furrow, a significantly expanded lateral trochlea, and a large lateral collateral ligament pit. The terminal phalanx is a robust, medially curved, claw-like ungual with a lateral groove only on the medial side. Metacarpal II is dumbbell-shaped; the proximal articular surface is flat and slightly pitted with a distally deflected medial margin to accommodate metacarpal I. The proximal articular surface is medially inclined and rectangular in outline. Phalanges II-1 and II-2 are short with well-developed laterally expanded trochleae and deep sagittal furrows that cause digit II to curve medially when articulated. Additionally, II-1 has a distal deflection on the palmar side of the proximal articular surface on the medial side that terminates in a lip, presumably a flexor tubercle. Digit II is terminated by a claw-like ungual that is curved slightly towards the palm with well-developed lateral grooves on both sides and is longer and more gracile than the ungual of digit I. Metacarpal III, like metacarpal II, is dumbbell-shaped and has a distally deflected medial margin on the proximal articular surface for articulation with digit II. Overall, it is more gracile than

metacarpal II. The phalanges of digit III are dorsoventrally compressed with moderately developed sagittal furrows and trochlea, and the digit is terminated by a small sesamoid-like distal ungual (OMNH 58340), rather than the clawed ungual that was previously reconstructed to terminate this digit (Forster, 1990:fig. 14 B; Dodson, 1980:fig. 1 D; Ostrom, 1970:plate 21 A). The sesamoid-like ungual is 10 mm long, 8 mm wide, and 5 mm proximo-distally, and is semi-ovoid, with a flat proximal surface and domed distal surface. The termination of digit III by a sesamoid-like ungual rather than a claw-like ungual may be an autapomorphy of *T. tilletti*. Other similarly well-known iguanodontian manus retain a clawed or hoof-like ungual on this digit (Galton, 1974; Gilmore, 1909; Norman, 1980). Metacarpal IV is short relative to metacarpals II and III, with a mediolaterally expanded proximal articular surface that is oval in outline and rounded on the margins. Like metacarpals II and III, the proximal condyle of metacarpal IV has a slight distal deflection on the medial side for articulation with metacarpal III. The distal condyle of metacarpal IV is rectangular in outline. Additionally, it has a well-developed collateral fossa on the medial and lateral side. Phalanx IV-1 is extremely short with a poorly defined trochlea and no sagittal furrow. Like digit III, digit IV is terminated by a sesamoid-like distal phalanx comparable to III-3 in size. The proximal and distal articular surfaces of metacarpal V are flared dorsally giving the dorsal side an arched appearance relative to the flat ventral side, as seen in other ornithischians such as, *Camptosaurus*, *Hypsilophodon*, *Leptoceratops*, and *Lesothosaurus* (Sereno, 1991). The extensively flared proximal margin is suggestive of a large degree of dorsiflexion between the carpus and metacarpals. Phalanx V-1 has a wide proximal articulation and a short distal condyle, with only one slightly-developed

trochlea. Like digits III and IV, digit V is terminated by a small sesamoid-like bone; this is missing from OMNH 58340 but present in OMNH 63525.

Discussion

The manus of *Tenontosaurus tilletti* retains plesiomorphic characteristics present in the manus of basal ornithischians (e.g. *Lesothosaurus* Galton, 1978) and basal ornithopods (e.g. *Hypsilophodon*). Digits I, II, and III, retain concavo-convex joints, sagittal furrows, sagittal crests, deep collateral ligament fossa, and prominent proximal processes for attachment of extensor and flexor tendons (Fig. 3). The concavo-convex articular surfaces, sagittal furrows and crests formed saddle-shaped joints in the phalanges of digits I-III that restricted motion to the sagittal plane and resisted torsion. When used during quadrupedal locomotion this type of joint is associated with a digitigrade posture (Moreno et al., 2007). Digits I, II, III were likely the primary digits used during locomotion; digits IV and V are extremely divergent laterally and lack the saddle-shaped joints. The divergent and reduced lateral digits are consistent with the general trend in Dinosauria to reduce the lateral digits (Sereno, 1997). The digits and metacarpals of *T. tilletti* lack the flattened articular surfaces associated with the shift to a sub-unguligrade manus posture, seen in ankylopollexians (a clade of derived iguanodontians with the synapomorphy of a fused or conical digit I). The metacarpals are short and dumbbell shaped like in *Hypsilophodon*, and lack the elongation and incipient tridactyl paring of digits II, III, and IV present in *Camptosaurus*, *Ouranosaurus* (Taquet, 1976) and taken to the extreme in *Iguanodon* (Fig 4). The claws terminating digits I and II are longer proximodistally than they are wide, in contrast to

the ungual of *I. bernissartensis* which are longer mediolaterally (hoof-like) (Norman, 1980).

The carpus, much like the phalanges, lacks ankylopollexian adaptations associated with weight bearing such as a row of distal carpal elements whose flattened surface permitted only small degrees of flexion, and an ossified carpal complex composed of the radiale, intermedium, and ulnare (Carpenter and Wilson, 2008). Additionally, the combined proximal surface of radiale, intermedium, and ulnare form distinct articular facets for articulation with the radius and ulna as seen in both *Camptosaurus dispar* and *Iguanodon bernissartensis* (Gilmore, 1909; Norman, 1980). The carpus of *Tenontosaurus* has three carpal elements that articulated slightly and possessed no incipient or well-developed articular facets for articulation with the radius and ulna, nor are there distal carpals present in any articulated specimens. Furthermore, shown most clearly by the articulated left manus of OMNH 58340, the carpals and metacarpals are not as closely associated as they are in *C. dispar* and *I. bernissartensis*; there is a gap varying from 7 mm (between the radiale and proximal surface of metacarpal I, to 30 mm (between the intermedium and proximal surface of metacarpal II; (Fig. 1). This positioning may suggest that there were extensive cartilaginous epiphyses present on the proximal articular surfaces of the metacarpals. Comparisons with extant archosaurs showed that dinosaurs, particularly sauropods and ornithischians, possessed extensive epiphyseal cartilage that formed a significant component of joint morphology in life. (Fujiwara et al., 2010; Holliday et al., 2010). The osseous signature of cartilaginous epiphyses is an undulating and pitted articular surface, which represents the inferred trace of vascular channels required to supply large cartilaginous structures (Holliday et

al., 2010). The proximal articular surfaces of the metacarpals of OMNH 58340 show the characteristic undulating surface texture described by Holliday et al. (2010) (Fig. 3C). This, coupled with the preserved space between the carpals and metacarpals, indicates that *T. tilletti* likely had extensive cartilaginous epiphyses filling the space between the carpals and metacarpals. The cartilage in the carpus may have acted as a shock-absorbing pad (Holliday et al., 2010) that preceded the evolution of a tightly articulating and ossified carpus as seen in other iguanodontian manus with weight-bearing adaptations (Gilmore, 1909; Norman, 1980).

Conclusions

The discovery of articulated manus of *Tenontosaurus tilletti* has provided multiple new insights into the manus morphology of this species: (1) the phalangeal formula is confirmed at 2-3-3-2-2 (based on OMNH 58340 and OMNH 63525), (2) digits III, IV, and V are now known to be terminated by small sesamoid-like distal phalanges that in disarticulated specimens were previously identified as distal carpal ossifications, (3) the lack of a clawed ungual on digit III is a deviation from the ornithischian primitive characteristic not seen in any other known iguanodontian manus and may be an autapomorphy of *Tenontosaurus tilletti*, and (4) the relationship of the carpals to metacarpals is suggestive of extensive cartilaginous epiphyses on the proximal articular surfaces of the metacarpals.

References

Brinkman, D. L., R. L. Cifelli, and N. J. Czaplewski. 1998. First occurrence of *Deinonychus antirrhopus* (Dinosauria: Theropoda) from the Antlers Formation (Lower Cretaceous: Aptian-Albian) of Oklahoma. Bulletin, Oklahoma Geological Survey, 146:1-27.

Boulenger, G. A. 1881. Sur l'arc pelvien chez les dinosauriens de Bernissart. Bulletins de l'Academie royale de Belgique, 1:600-608

Carpenter, K., and Y. Wilson. 2008. A new species of Camptosaurus (Ornithopoda: Dinosauria) from the Morrison Formation (Upper Jurassic) of Dinosaur National Monument, Utah, and a biomechanical analysis of its forelimb. Annals of Carnegie Museum, 76(4):227-263.

Cifelli, R. L., J. D. Gardner, R. L. Nydam, and D. L. Brinkman. 1997. Additions to the vertebrate fauna of the Antlers Formation (Lower Cretaceous), southeastern Oklahoma. Oklahoma Geology Notes, Oklahoma Geological Survey, 57:124-131.

Davis, B. M., R. L. Cifelli, and Z. Kielan-Jaworowska. 2008. Earliest Evidence Of Deltatheroida (Mammalia: Metatheria) From The Early Cretaceous Of North America, P. 3-24. *In* E. J. Sargis And M. Dagosto (Eds.), Mammalian Evolutionary Morphology: A Tribute To Frederick S. Szalay. Springer, Dordrecht.

Dodson, P. 1980. Comparative osteology of the American ornithopods *Camptosaurus* and *Tenontosaurus*. Mémoires de la Société Géologique de France, 139:81-85.

Forster, C. A. 1990. The postcranial skeleton of the ornithopod dinosaur *Tenontosaurus tilletti*. Journal of Vertebrate Paleontology, 10:273-294.

Fujiwara, S. I., H. Taru, and D. Suzuki. 2010. Shape of articular surface of crocodilian (Archosauria) elbow joints and its relevance to sauropsids. Journal of Morphology, 271(7):883-896.

Galton, P. M. 1974. The Ornitheschian Dinosaur *Hypsilophodon* from the Wealdon of the Isle of Wight. Trustees of the British Museum (Natural History). Geology, 25:1-152

Gilmore, C. W. 1909. Osteology of the Jurassic reptile *Camptosaurus*, with revision of the species of the genus and description of two new species. Proceedings of the United States National Museum, 36:197-332.

Hobday, D. K., C. M. Woodruff, and M. W. Mcbride. 1981. Paleotopographic and structural controls on non-marine sedimentation of the Lower Cretaceous Antlers Formation and correlatives, north Texas and southeastern Oklahoma. Society of Economic Paleontologists and Mineralogists, Special Publication, 31:71-87.

Holliday, C. M., R. C. Ridgely, J. C. Sedlmayr, and L. M. Witmer. 2010. Cartilaginous epiphyses in extant archosaurs and their implications for reconstructing limb function in dinosaurs. PLoS ONE, 5(9):e13120.

Huxley, T. On *Hypsilophodon*, a new genus of Dinosauria. Proceedings of the Geological Society of London, 204.

Jacobs, L. L., and D. A. Winkler. 1998. Mammals, archosaurs, and the Early to Late Cretaceous transition in north-central Texas, p. 253-280. *In* Y. Tomida, L. J. Flynn, and L. L. Jacobs (eds.), Advances in Vertebrate Paleontology and Geochronology. National Science Museum Monographs 14, Tokyo.

Manley, F. H. 1965. Clay Mineralogy and Clay-mineral Facies of the Lower Cretaceous Trinity Group, Southern Oklahoma: University of Oklahoma unpublished dissertation, 116 p.

Marsh, O. C. 1885. Names of extinct reptiles. American Journal of Science, 29(3):169.

Moreno, K., M. T. Carrano, and R. Snyder. 2007. Morphological changes in pedal phalanges through ornithopod dinosaur evolution: a biomechanical approach. Journal of Morphology, 268(1):50-63.

Norman, D. B. 1980. On the ornithischian dinosaur *Iguanodon bernissartensis* from the lower Lower Cretaceous of Bernissart (Belgium). Memoir de l'Institut Royal des Sciences Naturelles de Belgique, 178:1-105.

Norman, D. B. 2004. Basal Iguanodontia, p. 413-437. *In* David B. Weishampel, Peter Dodson, and Halszka Osmólska (eds.), The Dinosauria (Second Edition). University of California Press, Berkeley, California.

Ostrom, J. H. 1969. Osteology of Deinonychus antirrhopus, an unusual theropod from the Lower Cretaceous of Montana. Peabody Museum of Natural History, Yale University, 30.

Ostrom, J. H. 1970. Stratigraphy and paleontology of the Cloverly Formation (Lower Cretaceous) of the Bighorn Basin area, Montana and Wyoming. Peabody Museum of Natural History Bulletin, 35:1-234.

Rennison, C. J. 1996. The stable carbon isotope record derived from mid-Cretaceous terrestrial plant fossils from north-central Texas. Unpublished M.S. Thesis, Southern Methodist University, Dallas, 120 p.

Sereno, P. C. 1991. *Lesothosaurus*, "Fabrosaurids," and the early evolution of Ornithischia. Journal of Vertebrate Paleontology, 11(2):168-197.

Sereno, P. C. 1997. The origin and evolution of dinosaurs. Annual Review of Earth and Planetary Sciences, 25:435-489.

Taquet, P. 1976. Ostéologie d'Ouranosaurus nigeriensis, Iguanodontide du Crétacé Inférieur du Niger. Géologie et Paléontologie du Gisement de Gadoufaoua (Aptien du Niger), Chapitre, 3:57-168

Thomas, D. A. 2015. The cranial anatomy of *Tenontosaurus tilletti* Ostrom, 1970 (Dinosauria, Ornithopoda). Palaeontologia Electronica, 18.2.37A:1-99.

Werning, S. 2012. The ontogenetic osteohistology of *Tenontosaurus tilletti*. PLoS ONE, 7(3):e33539.

Winkler, D. A., P. A. Murry, and L. L. Jacobs. 1997. A new species of *Tenontosaurus* (Dinosauria: Ornithopoda) from the Early Cretaceous of Texas. Journal of Vertebrate Paleontology, 17(2):330-348.

Figures

Figure 1: The left manus of OMNH 58340 in a plaster support holder preserving the articulation as found, in palmar view.

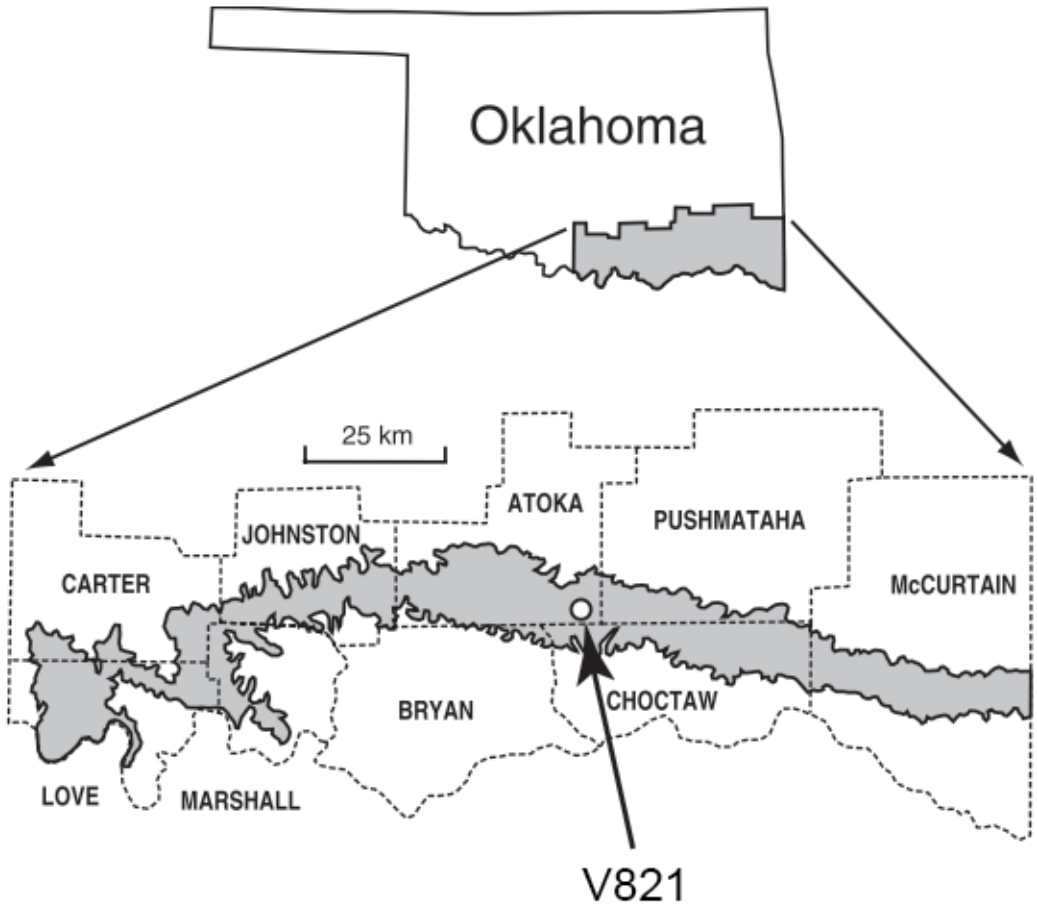

Figure 2: Map of southeastern Oklahoma depicting the area over which the Antlers formation outcrops in Oklahoma (shaded) and the location of OMNH locality V821 (modified from Davis et al., 2008).

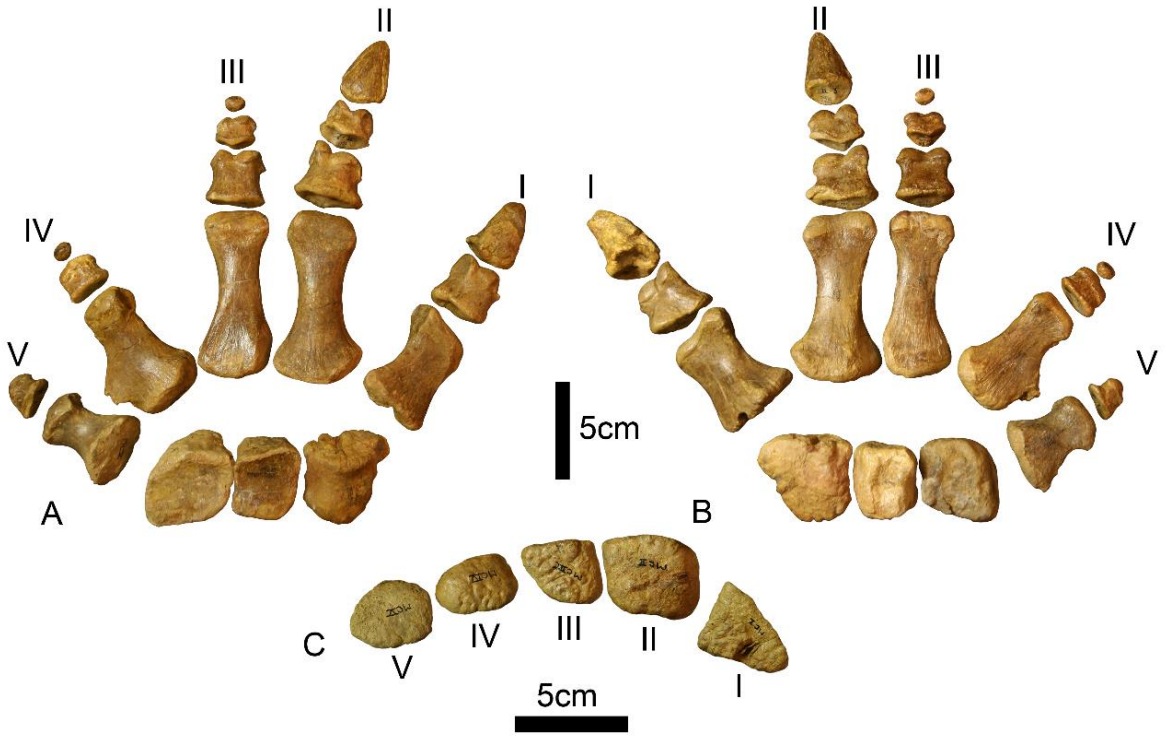

Figure 3: Left manus of OMNH 58340. **A.** Dorsal view **B.** Palmar view **C.** Proximal view of proximal articular surfaces.

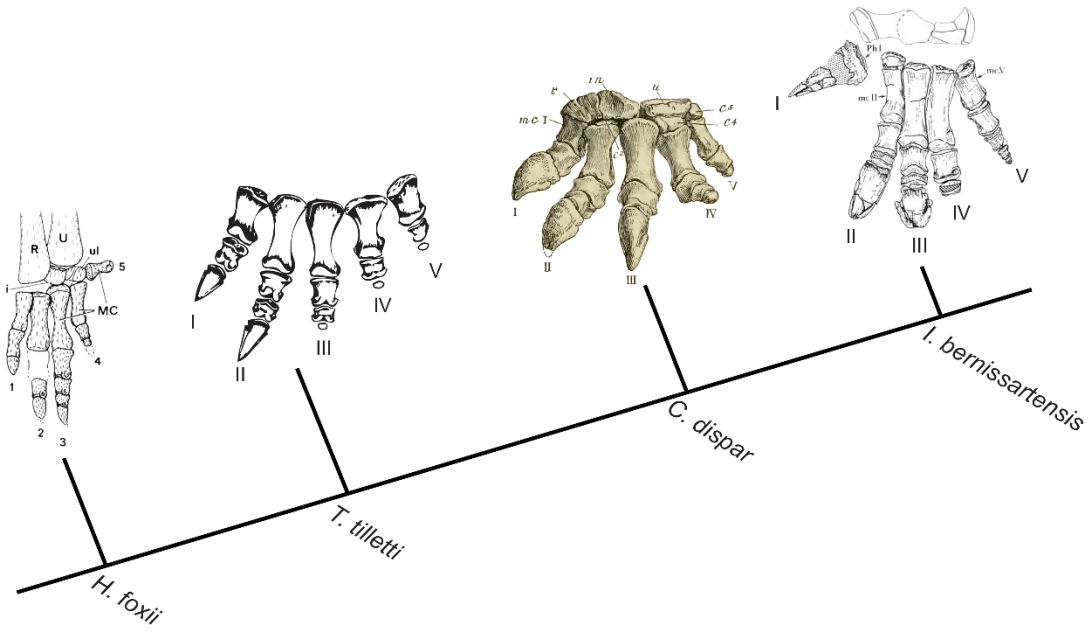

Figure 4: Manus phylogeny showing the change in manus shape in Iguanodonts (including representative left manus of *Tenontosaurus tilletti*, *Camptosaurus dispar*, *and Iguanodon bernissartensis*) with *Hypsilophodon foxii* representing basal ornithopod manus morphology (manus depictions adapted from Forster, 1990:fig 14; Galton, 1974:fig 41; Gilmore, 1909:fig 28; Norman, 1980:fig 60a)

First Documented Pathologies in *Tenontosaurus tilletti* with Comments on Infection in Non-Avian Dinosaurs

Introduction

In recent years, the field of dinosaurian paleopathology has grown significantly expanding the breadth of taxa involved and types of pathologies reported (Butler et al., 2013; Foth et al., 2015; Matthias et al., 2016; Peterson and Vittore, 2012; Senter and Juengst, 2016; D. Tanke and Rothschild, 2014; Tanke and Rothschild, 2010; Xing et al., 2018). Through this large data set it has become clear that while injuries or abnormalities are quite common and well-documented, demonstrable infection is not common in dinosaurs (Rega, 2012). In a review of 119 theropod pathologies, Molnar (2001) found only seven instances of infection. However, some large theropod skeletons (e.g., *Allosaurus fragilis* (see Foth et al., 2015; Hanna, 2002) and *Tyrannosaurus rex* (Molnar, 2001)) show multiple isolated cases of infection, a result of their active predatory lifestyle. In contrast, herbivorous dinosaurs typically only display single cases of infection (Gross et al., 1993; Lü et al., 2007; Xing et al., 2018) with rare instances of multiple infected elements (García et al., 2017; Tanke and Rothschild, 2014). Additionally, it has been suggested that non-avian dinosaurs do not exhibit hematogenous (blood-borne) osteomyelitis, due to the inferred similarities in their immune response with reptiles and their apparent ability to isolate osteomyelitis to single elements (Foth et al., 2015).

Here, I report five skeletal pathologies on a nearly complete subadult *Tenontosaurus tilletti* from the Antlers Formation of southeastern, Oklahoma. Prior reports of

pathologies and evidence of bone modification on T. tilletti skeletons include only feeding traces attributed to the predatory theropod *Deinonychus antirrhopus* (Ostrom, 1969), none of which contain evidence of healing and therefore are not considered pathologies (Brinkman et al., 1998; Gignac et al., 2010). The pathological bones observed in this study include: left dorsal ribs 7 and 10, right dorsal rib 10, left pedal phalanx I-1, and left metacarpal IV. The pathologies present on this individual represent three distinct cases of infection. Furthermore, the infection on metacarpal IV is consistent with the morphology of a Brodie abscess, which in humans is a type of osteomyelitis that is hematogenous in origin, indicating that hematogenous osteomyelitis affected non-avian dinosaurs.

Institutional abbreviations: BMR, Burpee Museum of Natural History, Rockford, Illinois, USA; FMNH, Field Museum of Natural History, Chicago, Illinois, USA; MOR, Museum of the Rockies, Montana State University, Montana, USA; OMNH, Sam Noble Museum of Natural History, Norman, Oklahoma, USA; TMP, Royal Tyrrell Museum of Palaeontology, Drumheller, Alberta, Canada; UMNH, Utah Museum of Natural History, University of Utah, Salt Lake City, Utah; UUVP, University of Utah Vertebrate Paleontology, Salt Lake City, Utah, USA (housed at UMNH)

Material & Methods

OMNH 58340 is a subadult *Tenontosaurus tilletti* collected from OMNH locality V821, during the 2000–2001 field season (Werning, 2012). V821 is located in Atoka County, Oklahoma, within the Aptian-Albian aged Antlers Formation (Jacobs and Winkler, 1998). In addition to OMNH 58340, the articulated vertebrae of the holotype specimen for *Sauroposeidon proteles* (Wedel et al., 2000) was collected 3-5m stratigraphically below OMNH 58340 at V821 (Thomas, 2015). OMNH 58340 is nearly

complete with only the mid-section of the tail missing due to weathering prior to discovery.

In total, OMNH 58340 has five pathological elements, two left ribs, a right rib, left pedal phalanx I-1, and the left metacarpal IV. Bone abnormalities were diagnosed through macroscopic inspection and with the aid of Computed Tomography (CT). Pathologies were classified as traumatic (from injury), infectious (from viral, bacterial, and fungal foreign agents), traumatic-infectious (infection following an injury), developmental (caused by growth disturbance during development), or idiopathic (the pathogenesis is indeterminate) (sensu Hana, 2002).

CT scans were performed at the University of Oklahoma Health Science Center using a Philips Brilliance 16 slice CT scanner. Metacarpal IV was scanned at 120 kVp and 151 mAs at 16 x 0.7mm slices and reconstructed at 0.35 mm overlapping slices with a high-resolution filter on a 512 matrix. Phalanx I was scanned at 120 kVp and 251 mAs at 16 x 0.7mm slices and reconstructed at 0.35 mm overlapping slices with a high-resolution filter on a 512 matrix. Ribs L7-L10, and R10 were scanned at 140 kVp and 199 mAs at 16 x 1 mm slices and reconstructed at 0.5 mm overlapping slices with a high-resolution filter on a 512 matrix. Data were exported as DICOM files representing a 69.0mm field of view and are available in the supplementary data files. Measurements of the circumference of phalanx-1 were taken macroscopically with a measuring tape, and measurements of endosseous structures were measured on the CT scans using the measure function in Fiji (Schindelin et al., 2012).

Results

Phalanx I-1

The left pedal phalanx I-1 has a large, irregularly shaped exostosis surrounding the diaphysis and the proximal articular surface (Fig. 5A–C). The surface of the exostosis is rugose and covered in shallow, irregular pits with multiple areas of raised bony spicules. The exostosis has increased the circumference of the diaphysis to be nearly equal to the circumference of the proximal articular surface. The inflation of the diaphysis is not uniform; the dorsal side shows more expansion than the plantar side, particularly on the dorsomedial edge (Fig. 5H). The exostosis surrounding the diaphysis at its widest extent has a circumference of 14.4 cm, whereas the unaffected right phalanx has a circumference of 8 cm. Proximal to distal condyle on the dorsal side, there is a pronounced lip terminating the extent of the exostosis, leaving the distal condyle unaffected. Deformation caused by the exostosis modified the articular surface with metatarsal I into a wide, ovate shape with no observable extensor tubercle (Fig. 5B). In contrast with the unaffected right phalanx I-1, the articular surface is overall more rounded, creating a pentagonal outline (Fig. 5E). Additionally, the shape of the fossa within the proximal articular surface of phalanx I-1 has been deformed from circular in outline to more elliptical and its depth has been elaborated by the growth of the exostosis (Fig. 5B, E).

In CT scan dorsal view, a faint, internal, dense line is observed one-third of the way down the shaft from the proximal end, indicating the presence of the original diaphyseal cortical bone. When outlined, the internal line conforms to the corresponding section of the diaphysis in the unaffected phalanx. The cortical bone can also be observed in the

proximal view and is present throughout the proximal two-thirds of the element. Based on the location of the original cortical bone, the primary expansion of the exostosis was in the dorsomedial direction. Additionally, the CT scans reveal this element to be taphonomically fractured to a degree atypical of other bones belonging to OMNH 58340. The fracturing present on the phalanx cross-cuts pathological features and therefore is most likely due to taphonomic processes (Fig. 5G-I). This could be the result of the pathology reducing the structural integrity of the phalanx.

Adjacent bones are unaffected, except for the distal condyle of metatarsal I. The proximal articular surface of left pedal phalanx I-1 is more concave than the unaffected contralateral phalanx I-1; therefore, the distal condyle of left metatarsal I was remodeled accordingly, resulting in a more convex articular surface than that of the right metatarsal I.

Diagnosis: This pathology bears a strong resemblance to that of two pedal phalanges belonging to *Allosaurus fragilis*, described by Hanna (2002). The right pedal phalanx III-1 of MOR 693 and the left pedal phalanx III-1 (UUVP 1657) of another *Allosaurus* from the Cleveland-Lloyd Quarry both possess a large exostosis covering the proximal two-thirds of the diaphysis and the proximal articular surfaces. The diaphyseal and articular expansions are interpreted as an involucrum— a periosteal outgrowth of bone that surrounds the original bone in response to an infection within the medullary cavity—that may have occurred secondarily to a trauma-related fracturing of these elements. Therefore, a combination of callus formation and infection-related bone growth could have produced these abnormalities. Both specimens possess what Hanna (2002) interpreted to be penetrating lesions, cloacae for the drainage of pus produced in

response to osteomyelitis, on the exterior of these phalanges. The penetrating lesions and involucrum are interpreted as evidence of infection and therefore Hanna (2002) classified these pathologies as post-traumatic chronic suppurative osteomyelitis. Rega (2012) challenged this diagnosis suggesting that the phalanx I-1 of MOR 693 lacks cloacae and that the surface texture and inflation of the element could be indicative of a benign bone tumor called an osteochondroma. Therefore, a differential diagnosis of OMNH 58340 phalanx I-1 should discuss three possible etiologies: an osteochondroma, callus formation, and osteomyelitis.

Osteochondromas are the most common bone tumors found in humans (Murphey et al., 2000). They are characterized as benign outgrowths that consist of medullary and cortical bone capped by hyaline cartilage. The pathognomonic characteristic of this type of lesion is its continuity with the underlying non-pathological bone cortex (Murphey et al., 2000). Therefore, in diagnosing an osteochondroma it is crucial to determine if the exostosis is in continuity with the cortical bone and underlying medullary cavity. The presence of the original cortical bone (Fig. 5G, H) within the exostosis strongly argues against a diagnosis of an osteochondroma for this element, because the exostosis is not continuous with the original cortical and medullary cavity. Osteochondromas do not typically envelope the bone they outgrow from, rather this morphology is more consistent with either callus formation or osteomyelitis.

The latter etiologies are not mutually exclusive; callus formation can begin, and bacteria can be introduced secondarily causing osteomyelitis. Internally, there is no evidence of a malunion of the cortical bone within the phalanx; however, this may be obscured by the beam hardening caused by iron-bearing permineralization. Alternatively, the lack of

resolution surrounding the cortical bone may reflect a callus in the later stages of healing, where osteoclastic activity has begun resorbing the original cortical bone (Straight et al., 2009). This inference may be corroborated by the fact that the left metatarsal I has a more convex distal articular surface, to match the increased concavity of the pathological proximal articular surface on the phalanx, a degree of remodeling that would indicate a significant span of time has passed. The rough, pitted texture covering the callus appears similar to the texture associated with osteomyelitis in a sauropod tail in which the periosteal surfaces of multiple caudal vertebrae were covered with a rough 'microbubbly' surface texture (García et al., 2017). Therefore, the rugose texture of the periosteal surface surrounding the phalanx is consistent with osteomyelitis and this element's pathology is considered traumatic-infectious (Hanna, 2002).

Ribs

Left dorsal rib 7 (L7) is fractured just below the greatest curvature of the rib, 75 mm distal to the tuberculum (Fig 6B). The distal portion of the rib is compressed and telescoped approximately 14.5 mm proximally into the broken end of the proximal rib segment, resulting in a total shortening of 26 mm. The ventral side of the rib is cracked and bulged outward to accommodate the impaction of the distal rib segment into the proximal rib segment. There are no signs of callus formation surrounding the break. The CT scans (Fig. 6C, D) of this pathology clearly show stacked cortical bone on the ventral side of the rib.

Right dorsal rib 10 (R10) is fractured 140 mm below the tuberculum where the rib begins to straighten out. The distal end of the fracture is displaced 18 mm proximally (Fig. 6A), for a total shortening of the rib by 24 mm. While still an impacted fracture

the morphology differs slightly from that of L7. There is minor angulation of the distal rib segment so that the anterior cortical bone the of distal rib segment overlays the anterior cortical bone of the proximal rib segment. Furthermore, some deformation and cracking is present on the ventral side like what is seen in L7. There is no callus formation around the break.

Left dorsal rib 10 (L10) has a smooth, inflated callus 35 mm below the tuberculum (Fig. 7). There is no visible offset, nor is there any indication of a fracture except the extensive callus. The callus is demarcated from the non-pathological bone by an eye-shaped texture change 22 mm long (proximodistally) and spanning the width of the rib. The callus expands the circumference of the bone from 55 mm distal to the callus to 67 mm at the widest point of the callus. On the anterior surface of the callus, there are two small erosive lesions with sharp edges that pass through the periosteal surface of the callus. The distal lesion is heart-shaped, 9 mm by 7 mm in size and 2-3 mm deep. The proximal lesion is smaller in size (5 mm by 5 mm) and is not as deep as the distal lesion (Fig. 7B). The lesions are located within the eye-shaped margin of the callus.

Diagnosis: Ribs L7 and R10 are classified as traumatic. The two rib fractures are consistent with direct trauma to the rib cage. The impact direction can be inferred from the location of the fractures on the ribs. A fracture at or near the angle of the rib is indicative of a force applied from the ventral side of the rib cage, for example from a fall (Lovell, 1997). Multiple aspects suggest that the fractures of L7 and R10 are from the same traumatic event. L7 and R10 are both impacted fractures with 26 mm and 24mm of impaction, respectively, indicating an equivalent force fractured both ribs. Additionally, both ribs have no external or visible internal callus formation, indicating

that the fractures were likely synchronous. The lack of healing is permissive of two interpretations: (1) that these fractures occurred perimortem; (2) that the rib fractures occurred postmortem. Two features of these fractures support the former hypothesis. The fractures, particularly on the ventral sides of the ribs, are consistent with the breaking of pliable living bone, rather than the brittle fracturing of weathered or permineralized bone, wherein soft tissue (such as collagen) is lacking. Furthermore, the similar degree of impaction on L7 (26mm) and R10 (24 mm) when no other ribs were affected by such force, argues against taphonomic (postmortem) deformation.

Rib L10 is classified as traumatic-infectious. The presence of a callus or proliferative lesion is necessary but not sufficient to diagnose a pathology as traumatic (Rega, 2012). Additional factors such as location and type of lesion need to be considered. The callus on L10 (Fig. 7A) is at the greatest curvature of the rib, again indicative of a force from the ventral side of the rib cage (Lovell, 1997). The smooth callus is most prominent on the anterior side, and the CT scans reveal no internal cortical bone, all of which are consistent with a rib fracture in the later stages of callus remodeling (Rega, 2012). The lytic lesions present on the anterior side of the callus are localized areas of bone destruction characteristic of osteomyelitis in reptiles and mammals (Antinoff, 1997; Ortner, 2003). The morphology of lytic lesions can be used to determine the rate of bone destruction within. If the bone lysis ceases after an initial phase of destruction, the lesion will be circumscribed by bony sclerosis. However, if lysis is still active and progressing at a moderate pace, the margins of the lesion will be sharply defined with no sclerosis. If lysis is progressing at a rapid pace, the margins of the lesion will exhibit a gradient of destruction rather than a sharply defined margin. The heart-shaped lesion

has internal margins that are sharply defined with no apparent sclerotic bone formation; therefore, this lesion was progressing at a moderate rate of bone destruction (Fig. 7B). The margins of the more proximal lesion are extremely irregular. This may be caused by the lack of complete penetration of the cortical bone of the callus or it may signify that lysis in this lesion was progressing at a higher rate (Ortner, 2003). Thus, the lytic lesions present on the external surface of this callus indicates that there was either an infection in the surrounding soft tissue or that the infection had spread to the bone and was progressing into a chronic phase of osteomyelitis.

Metacarpal IV

A large exostosis is present 10 mm beyond the proximal articular surface on the lateral side of the diaphysis. The exostosis begins to diverge from the lateral side of the shaft 30 mm from the distal condyle forming a sub-triangular outgrowth that projects laterally 20 mm from the lateral side of the bone (Fig. 8A). The termination of the exostosis is rugose and composed of cortical bone. There is no abnormal bone thickening in the dorsal and palmar directions; rather the exostosis appears to continue the normal periosteal surface of the bone on the dorsal and palmar sides. However, on the dorsal side, there is a concentric disruption of the normal long grain bone texture, 20 mm in diameter, coinciding with an underlying intraosseous abscess (Fig. 8C–E). The texture within the disruption is completely disorganized. In addition to the large exostosis, there is a small bone spicule 3 mm in length extending laterally from the proximal margin of the lateral collateral ligament pit. The proximal and distal epiphyses are unaffected.

Computed Tomography (CT) scans of metacarpal IV were crucial in characterizing the internal morphology of this pathology. These CT scans reveal that within the exostosis

there is an internal abscess that measures 11.5 X 9.2 X 6.2 mm (Length X Width X Height) that is ovoid in shape with the long axis oriented palmodorsally. The lesion is in the medullary cavity of the diaphysis 6 mm distal the proximal condyle and just within the cortical bone on the lateral side. The margin of the abscess is clear and distinct, with a dense rim of cancellous sclerosis circumscribing the abscess. Contained within the abscess is an irregularly-shaped sequestrum. The sequestrum mimics the abscess in shape and has a density consistent with the surrounding bone, eliminating the possibility that it is a diagenetic mineral filling the void created by the abscess. Additionally, the exostosis is as it appears macroscopically, is a well-organized periosteal outgrowth composed internally of cancellous bone and externally of cortical bone.

Diagnosis: The exostosis on metacarpal IV is interpreted as a periosteal response to the proliferation of an internal abscess and therefore is considered one pathology. The morphology of the metacarpal IV abnormality is consistent with the characteristics of a Brodie abscess, a type of subacute pyogenic osteomyelitis, therefore this pathology is classified as infectious. Brodie abscesses are variable in humans in terms of size, degree of osseous proliferative response, and location. Because of their variability, they are commonly misdiagnosed (Miller et al., 1979). Their typical imaging appearance is characterized as an intraosseous bone lesion with an eccentric area of bone destruction that is variably emarginated by reactive sclerosis of the surrounding bone. In a study of 25 confirmed cases of Brodie abscesses in humans, all but one occurred in the lower limbs, most commonly in the tibia and the femur (Miller et al., 1979). Nine were present in the diaphysis and of those nine, four were in the medullary cavity. In all but four cases, cancellous sclerosis was present surrounding the abscess, and in ten of the

cases, reactive periosteal growth like that of the exostosis on metacarpal IV was present. Sequestrum was present in five of the 25 cases and the authors suggested that presence of sequestra may indicate an abscess early in its development (Miller et al., 1979). A differential diagnosis including a Brodie abscess must also include a discussion of the characteristics of an osteoid osteoma, a type of benign bone tumor (Atesok et al., 2011). An osteoid osteoma produces a morphology that is similar to a Brodie abscess in CT scans, including a low attenuation nidus (hole) and adjacent sclerosis of the surrounding bone (Atesok et al., 2011). However, irregular sequestra like that seen within the abscess on the metacarpal IV of *Tenontosaurus* is not typical of an osteoid osteoma; rather a central mineralization may be present within the nidus of the osteoid osteoma, but is spheroidal (Atesok et al., 2011; Vittore and Henderson, 2013). The abscess within metacarpal IV of OMNH 58340 exhibits many of the characteristics associated with Brodie abscesses, including; (1) a cancellous sclerotic rim that surrounds the area of bone destruction (Fig. 8C, D), (2) a reactive periosteal outgrowth closely associated with the abscess; and (3) an eccentric, irregularly shaped sequestrum typical of early-stage hematogenous osteomyelitis (Fig. 8C–E). Moreover, a diagnosis of this pathology is not unprecedented in non-avian dinosaurs. A Brodie abscess was described by Vittore and Henderson (2013) in the left pedal phalanx II-1 of the tyrannosaurid BMR P2002.4.1. However, this is the first reported Brodie abscess in herbivorous dinosaurs.

Discussion

The five pathologies diagnosed herein for the skeleton of *T. tilletti* (OMNH 58340) are classified following Hanna (2002) as follows: left dorsal rib 7 (L7) and right dorsal rib 10 (R10) are traumatic, the left pedal phalanx I-1 and left dorsal rib 10 (L10) are traumatic-infectious, and the left metacarpal IV is infectious. The pathologies present on this individual suggest a minimum of two traumatic events. The pathologies on left phalanx I-1 and L10 appear to be in the late stages of callus remodeling, suggesting they are contemporaneous injuries likely related to a fall on the left side. The lack of healing, similar fracture location, type, and extent of fracture to ribs L7 and R10 strongly suggest that these injuries are contemporaneous and occurred perimortem. The development of the Brodie abscess is difficult to constrain directly; the recurrent dull ache associated with a Brodie abscess has been reported to last from four weeks to ten years in humans. Therefore it is possible the Brodie abscess preceded all other injuries present on OMNH 58340 (Brodie, 1832; Miller et al., 1979). However, the extensive sequestra within the Brodie abscess indicates that it might be early in its development, potentially placing its development around the time of the initial trauma event (Miller et al., 1979).

In isolation, the symptoms of these pathologies are unlikely to be immediately fatal, yet the sum may have directly contributed to this individual's death. The fractures present on phalanx I-1 and L10 would have caused localized swelling and chronic pain, although the post-traumatic osteomyelitis likely had greater systemic effects. Fighting infection such as osteomyelitis requires a strong immune response, thus demanding an increased intake of food and fluids (Gross et al., 1993). The symptoms of a Brodie

abscess are generally isolated to the affected limb and include a dull recurrent ache, local swelling, and in some patients a pronounced limp (Brodie, 1832; Miller et al., 1979). Therefore, the Brodie abscess present in metacarpal IV, in combination with the osteomyelitic phalanx, may have inhibited this animal's ability to acquire food resulting in malnutrition and a suppressed immune system leaving it susceptible to greater secondary infection (Gross et al., 1993). The impacted fractures of R10 and L7 likely directly contributed to the death of this animal as evident from the lack of callus formation around the fractures. The fracture type, an impacted fracture, and the location of these fractures strongly suggest that this individual suffered a strong ventral force to the rib cage, suggestive of a fall. The impacted fractures shortened the ribs by 24 and 26 millimeters. Fractures of this type likely severed or injured the intercostal vessels and nerves that track along the inner curvature of the ribs. Following the severing of the vessels, hemothorax (the presence of blood within the thorax) may have developed due to internal bleeding (Lovell, 1997). Thus, this individual likely died from complications of its multiple injuries.

Osteomyelitis such as a Brodie abscess forms when pyogenic bacteria enters the bone via three possible vectors: (1) transmission through the infection of adjacent soft tissue, (2) direct transmission into the bone (e.g. through a compound fracture) and (3) transmission through the bloodstream (hematogenously) from another septic source (Ortner, 2003). While the condition of the soft tissue adjacent to the metacarpal IV is unknown, the Brodie abscess in metacarpal IV shows no evidence of trauma, therefore direct transmission is unlikely. In humans, hematogenous transmission is the most common vector of development and therefore is considered the method of transmission

for this pathology (Miller et al., 1979). In many cases, the septic source for a Brodie abscess cannot be identified. In a case study of 25 Brodie abscesses only 5 patients reported prior instances of infection varying from a staphylococcal abscess of the arm to blood poisoning (Miller et al., 1979). Other suggested septic sources include skin abscesses, infections of the genitourinary, gastrointestinal, biliary, and respiratory systems (Vittore and Henderson, 2013). Therefore, antecedent infection in the soft tissues should always remain a possible septic source of bacteria when looking at sources of infection in the fossil record. In the only other reported case of a Brodie abscess in non-avian dinosaurs, in which concomitant infected elements were lacking on the remains of a tyrannosaurid BMR P2002.4.1, Vittorre and Henderson (2013) suggested that dental trauma may have been the septic source of bacteria for the Brodie abscess on phalanx II-1 of BMR P2002.4.1. Dental trauma is well documented in theropods but is less likely to be the septic source in herbivorous dinosaurs, owing to the decreased chance of injury associated with an herbivorous feeding style. The most likely septic source for the Brodie abscess in OMNH 58340 is the infections present in phalanx I-1 and rib L10; however, because the state of soft tissue in this individual cannot be assessed, infection in the soft tissues cannot be ruled out.

Multiple studies have shown the utility of micro-CT and CT scanning as a non-invasive way of studying the internal morphology of bones (Anné et al., 2015; Straight et al., 2009; Vittore and Henderson, 2013). The application of CT scanning in this diagnosis was integral for narrowing the range of possible etiologies. The identification of the original cortical bone within the callus on phalanx I-1 was crucial in differentiating between a diagnosis of an osteochondroma—which had been suggested for similar

structures on MOR 693 and UUVP 1657—and a callus with a post-traumatic infection (Hanna, 2002). Furthermore, prior to CT scanning, the morphology of the metacarpal IV abnormality was consistent with tendon avulsion, stress fracture, osteochondroma, and enthesopathy. The visualization of an internal abscess through CT reduced the differential diagnosis to two possibilities: a Brodie abscess and an osteoid osteoma. The CT scans revealed that the pathology was consistent with a Brodie abscess, confirming the second report of hematogenous osteomyelitis in non-avian dinosaurs and the first report in Ornithopoda. Future study methods should include CT scanning as a diagnostic tool, especially if the pathological elements in question are located in the axial skeleton, where hematogenous osteomyelitis is most likely to occur (Emslie and Nade, 1983; Miller et al., 1979; Ortner, 2003; Vittore and Henderson, 2013).

The presence of hematogenous osteomyelitis, in the form of a Brodie abscess, in this individual and BMR P2002.4.1 suggests that the hematogenous spread of infection in dinosaurs may be more common than previously recognized (Vittore and Henderson, 2013). Foth et al. (2015) used the lack of hematogenous osteomyelitis and the isolation of infection to single elements in *Allosaurus* to suggest that extant phylogenetic bracketing should be applied in pathological studies and a reptilian-immune response should be considered for dinosaurs, while mammalian comparisons should be avoided. This is based on the differing physiological responses to infection present in mammals, birds, and reptiles. Upon infection by pyogenic organisms, reptiles and birds produce a caseous substance called fibrin. If the infection continues or does not rupture to the surface, a hard, encapsulating mass forms around the focus of infection, called a fibriscess (Huchzermeyer and Cooper, 2000; Mader, 2006). The isolation of a pathogen

in a fibriscess appears to restrict the spread of infection, reducing the likelihood of septicemia in birds and reptiles (Huchzermeyer and Cooper, 2000). In contrast, mammals produce pus at the focus of an infection, forming a suppurative abscess by which adjacent tissues are more likely to be affected, with an increased chance of septicemia relative to reptiles (Ortner, 2003). The pathologies on OMNH 58340 do not show dissemination to adjacent bones, consistent with the observation of infected element in *Allosaurus* and other dinosaurs, yet the Brodie abscess is undoubtedly hematogenous in origin (Foth et al., 2015; Gross et al., 1993; Hanna, 2002; Rega, 2012; Senter and Juengst, 2016). The presence of hematogenous osteomyelitis may indicate that a more avian-like immune response to infection should be considered for dinosaurs because, although rare in birds, birds do exhibit hematogenous osteomyelitis (Emslie and Nade, 1983; Maier et al., 2015).

When describing pathologies, previous investigators have chose to use a mammalian model, particularly in reference to infection (Gross et al., 1993; Hanna, 2002; Rega, 2012; Vittore and Henderson, 2013; Xing et al., 2018). This is likely due to two reasons; first, there is abundant literature on mammalian pathologies owing to an anthropocentric bias in medical literature, and second, infectious pathologies in dinosaurs bear a strong resemblance to mammalian infectious pathologies. Rega (2012) noted that the morphology of an abnormality on the fibula of a *Tyrannosaurus rex*, FMNH PR 2018 has an involucrum, sequestrum, and cloaca, all suggestive of a mammalian pus producing reaction. However, the described morphology does not necessitate that dinosaurs produced pus; rather, it suggests that the response to osteomyelitis in dinosaurs and mammals might produce the same osseous morphology.

Two studies—Emslie and Nade (1983), and Tully et al. (1996)—noted that osteomyelitis in birds follows a similar pathogenesis to mammals and can produce similar osseous responses in analogous elements. Tully et al. (1996) described osteomyelitis in the tarsometatarsus of two ratites, both of which exhibit a sequestrum and involucrum. The radiographs of an ostrich show an involucrum, sequestrum, and a small sinus tract (cloaca) draining liquid exudate through a fistula in the skin, characters commonly associated with mammalian osteomyelitis. Tully et al. (1996) noted that the presence of sequestra in ratites bears a strong resemblance to sequestra commonly found in infected metacarpals and metatarsals of horses. These examples indicate that mammalian descriptors and diagnoses might not be wholly inapplicable when describing dinosaurian infection as some researchers have suggested (Foth et al., 2015; Senter and Juengst, 2016). The similarity in osseous response to infection in birds and mammals should be the subject of future studies to better inform descriptions of infectious pathologies in dinosaurs. Owing to the similarities between birds and mammals discussed above, and the similarities in morphology of our specimen with the characteristics of a mammalian Brodie abscess, we chose to use mammalian descriptors when diagnosing the internal abscess present in metacarpal IV. We implore future researchers to consider use of mammalian descriptors when describing infection if such descriptors appear to accurately describe the morphology of the infection.

References

Anné, J., R. J. Garwood, T. Lowe, P. J. Withers, and P. L. Manning. 2015. Interpreting pathologies in extant and extinct archosaurs using micro-CT. PeerJ, 3:e1130.

Antinoff, N. 1997. Osteomyelitis in reptiles. Proceedings Association of Reptilian and Amphibian Veterinarians. Houston (TX): ARAV, 4:149-152.

Atesok, K. I., B. A. Alman, E. H. Schemitsch, A. Peyser, and H. Mankin. 2011. Osteoid osteoma and osteoblastoma. JAAOS-Journal of the American Academy of Orthopaedic Surgeons, 19(11):678-689.

Brinkman, D. L., R. L. Cifelli, and N. J. Czaplewski. 1998. First occurrence of *Deinonychus antirrhopus* (Dinosauria: Theropoda) from the Antlers Formation (Lower Cretaceous: Aptian-Albian) of Oklahoma. Bulletin, Oklahoma Geological Survey, 146:1-27.

Brodie, B. C. 1832. An account of some cases of chronic abscess of the tibia. Medico-chirurgical transactions, 17:239.

Butler, R. J., A. M. Yates, O. W. M. Rauhut, and C. Foth. 2013. A pathological tail in a basal sauropodomorph dinosaur from South Africa: evidence of traumatic amputation? Journal of Vertebrate Paleontology, 33(1):224-228.

Emslie, K. R., and S. Nade. 1983. Acute hematogenous staphylococcal osteomyelitis. A description of the natural history in an avian model. The American journal of pathology, 110(3):333.

Foth, C., S. W. Evers, B. Pabst, O. Mateus, A. Flisch, M. Patthey, and O. W. Rauhut. 2015. New insights into the lifestyle of Allosaurus (Dinosauria: Theropoda) based on another specimen with multiple pathologies. PeerJ, 3:e940.

García, R. A., I. A. Cerda, M. Heller, B. M. Rothschild, and V. Zurriaguz. 2017. The first evidence of osteomyelitis in a sauropod dinosaur. Lethaia, 50(2):227-236.

Gignac, P. M., P. J. Makovicky, G. M. Erickson, and R. P. Walsh. 2010. A description of Deinonychus antirrhopus bite marks and estimates of bite force using tooth indentation simulations. Journal of Vertebrate Paleontology, 30(4):1169-1177.

Gross, J., T. Rich, and P. Vickers-Rich. 1993. Dinosaur bone infection. RESEARCH & EXPLORATION, 9(3):286-293.

Hanna, R. R. 2002. Multiple Injury and Infection in a Sub-Adult Theropod Dinosaur Allosaurus fragilis with Comparisons to Allosaur pathology in the Clevland-Lloyd Quarry Collection. Journal of Vertebrate Paleontology, 22(1):76-90.

Huchzermeyer, F. W., and J. E. Cooper. 2000. Fibriscess, not abscess, resulting from a localised inflammatory response to infection in reptiles and birds. Veterinary Record, 147(18):515-517.

Jacobs, L. L., and D. A. Winkler. 1998. Mammals, archosaurs, and the Early to Late Cretaceous transition in north-central Texas, p. 253-280. *In* Y. Tomida, L. J. Flynn, and L. L. Jacobs (eds.), Advances in Vertebrate Paleontology and Geochronology. National Science Museum Monographs 14, Tokyo.

Lovell, N. C. 1997. Trauma analysis in paleopathology. American Journal of Physical Anthropology, 104(S25):139-170.

Lü, J., Y. Kobayashi, Y. N. Lee, And Q. Ji. 2007. A new Psittacosaurus (Dinosauria: Ceratopsia) specimen from the Yixian Formation of western Liaoning, China: the first pathological psittacosaurid. Cretaceous Research, 28(2):272-276.

Mader, D. R. 2006. Chapter 42 - Abscesses, p. 715-719, Reptile Medicine and Surgery (Second Edition). W.B. Saunders, Saint Louis.

Maier, K., D. Fischer, A. Hartmann, O. Kershaw, E. Prenger-Berninghoff, H. Pendl, M. J. Schmidt, and M. Lierz. 2015. Vertebral Osteomyelitis and Septic Arthritis Associated With Staphylococcus hyicus in a Juvenile Peregrine Falcon (Falco peregrinus). Journal of Avian Medicine and Surgery, 29(3):216-223.

Matthias, A. E., L. A. Mcwhinney, and K. Carpenter. 2016. Pathological pitting in ankylosaur (Dinosauria) osteoderms. International Journal of Paleopathology, 13:82-90.

Miller, W. B., W. A. Murphy, and L. A. Gilula. 1979. Brodie abscess: reappraisal. Radiology, 132(1):15-23.

Molnar, R. 2001. Theropod paleopathology: a literature survey. Mesozoic Vertebrate Life:337-363.

Murphey, M. D., J. J. Choi, M. J. Kransdorf, D. J. Flemming, and F. H. Gannon. 2000. Imaging of osteochondroma: variants and complications with radiologic-pathologic correlation. Radiographics, 20(5):1407-1434.

Ortner, D. J. 2003. Identification of pathological conditions in human skeletal remains (Second Edition). Academic Press, San Diego.

Ostrom, J. H. 1969. Osteology of Deinonychus antirrhopus, an unusual theropod from the Lower Cretaceous of Montana. Peabody Museum of Natural History, Yale University, 30.

Peterson, J. E., and C. P. Vittore. 2012. Cranial pathologies in a specimen of Pachycephalosaurus. PLoS ONE, 7(4):e36227.

Rega, E. 2012. Disease in Dinosaurs, p. 667-711, The Complete Dinosaur. Indiana University Press.

Schindelin, J., I. Arganda-Carreras, E. Frise, V. Kaynig, M. Longair, T. Pietzsch, S. Preibisch, C. Rueden, S. Saalfeld, B. Schmid, J.-Y. Tinevez, D. J. White, V. Hartenstein, K. Eliceiri, P. Tomancak, and A. Cardona. 2012. Fiji: an open-source platform for biological-image analysis. Nature Methods, 9:676.

Senter, P., and S. L. Juengst. 2016. Record-Breaking Pain: The Largest Number and Variety of Forelimb Bone Maladies in a Theropod Dinosaur. PLoS ONE, 11(2):e0149140.

Straight, W. H., G. L. Davis, H. C. W. Skinner, A. Haims, B. L. Mcclennan, and D. H. Tanke. 2009. Bone lesions in hadrosaurs: Computed Tomographic Imaging as a guide for paleohistologic and stable-isotopic analysis. Journal of Vertebrate Paleontology, 29(2):315-325.

Tanke, D., and B. Rothschild. 2014. Paleopathology in Late Cretaceous Hadrosauridae from Alberta, Canada, p. 540-571, Hadrosaurs. Edited by D. A. Eberth and D. C. Evans. Indiana University Press, Bloomington, IN.

Tanke, D. H., and B. M. Rothschild. 2010. Paleopathologies in Albertan ceratopsids and their behavioral significance, 355-384 p.

Thomas, D. A. 2015. The cranial anatomy of *Tenontosaurus tilletti* Ostrom, 1970 (Dinosauria, Ornithopoda). Palaeontologia Electronica, 18.2.37A:1-99.

Tully, T. N., G. S. Martin, P. F. Haynes, J. Cornick-Seahorn, and R. D. Pechman. 1996. Tarsometatarsal Sequestration in an Emu (Dromaius novaehollandiae) and an Ostrich (Struthio camelus). Journal of Zoo and Wildlife Medicine, 27(4):550-556.

Vittore, C. P., and M. D. Henderson. 2013. Brodie Abscess Involving a Tyrannosaur Phalanx: Imaging and Implications, p. 223-237, Tyrannosaurid Paleobiology. Indiana University Press.

Wedel, M. J., R. L. Cifelli, and R. K. Sanders. 2000. *Sauroposeidon proteles*, a new sauropod from the Early Cretaceous of Oklahoma. Journal of Vertebrate Paleontology, 20:109-114.

Werning, S. 2012. The ontogenetic osteohistology of *Tenontosaurus tilletti*. PLoS ONE, 7(3):e33539.

Xing, L., B. M. Rothschild, P. S. Randolph-Quinney, Y. Wang, A. H. Parkinson, and H. Ran. 2018. Possible bite-induced abscess and osteomyelitis in Lufengosaurus (Dinosauria: sauropodomorph) from the Lower Jurassic of the Yimen Basin, China. Scientific Reports, 8(1):5045.

Figures

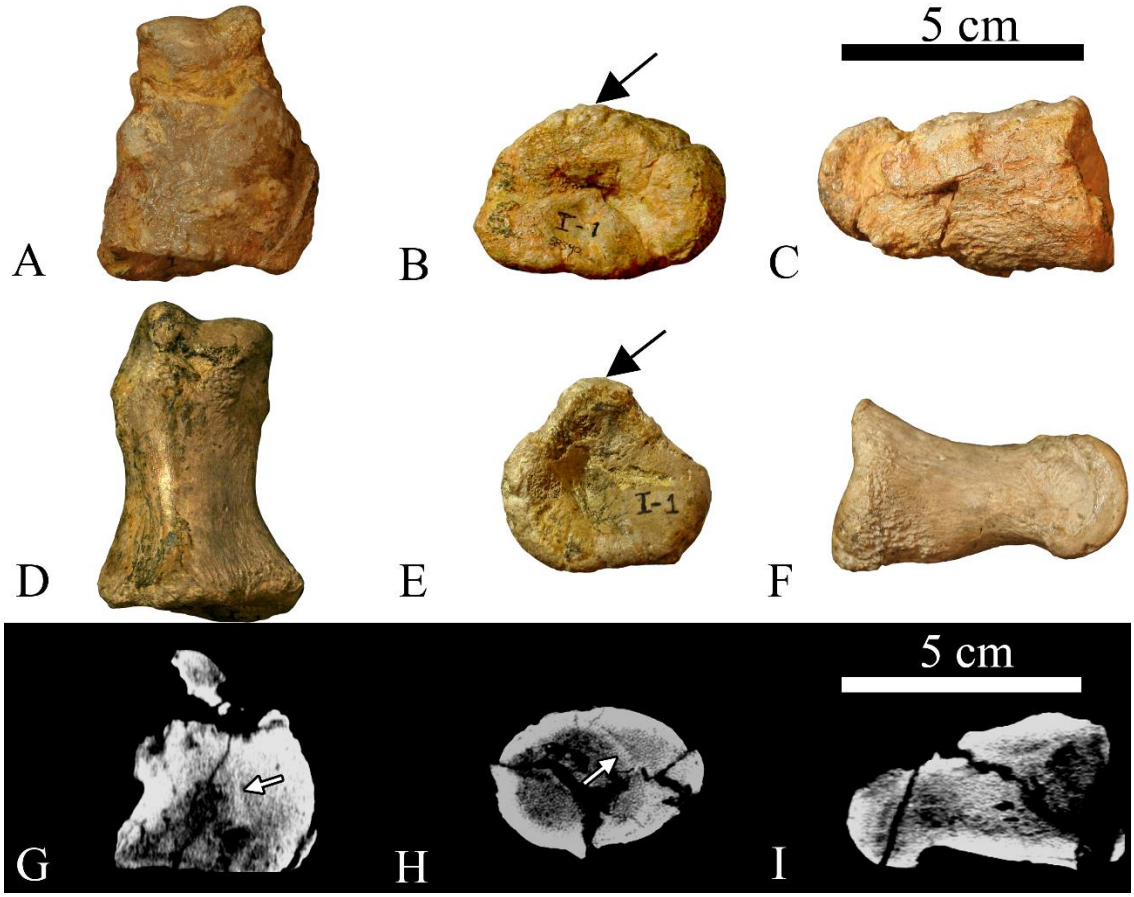

Figure 1: OMNH 58340 left pedal phalanx I-1 **(A-C, G-I)** and non-pathological right pedal phalanx I-1**(D-F)** for comparison. **(A, D, H**) dorsal view. **(B, E, I**) proximal view. **(C, F, J)** lateral view. The rugose callus has thickened the diaphysis and drastically changed the shape of the proximal articular surface. The black arrows denote the location of the extensor tubercle and the degree to which callus growth on the pathological specimen has obscured or remodeled the tubercle. The white arrows indicate original bone cortex surrounded by a mottled layer (woven bone) and a thin solid white layer (lamellar bone) this morphology is consistent with callus formation. The rough outer texture of the callus indicates that this element was secondarily affected by osteomyelitis (a traumatic-infectious pathology).

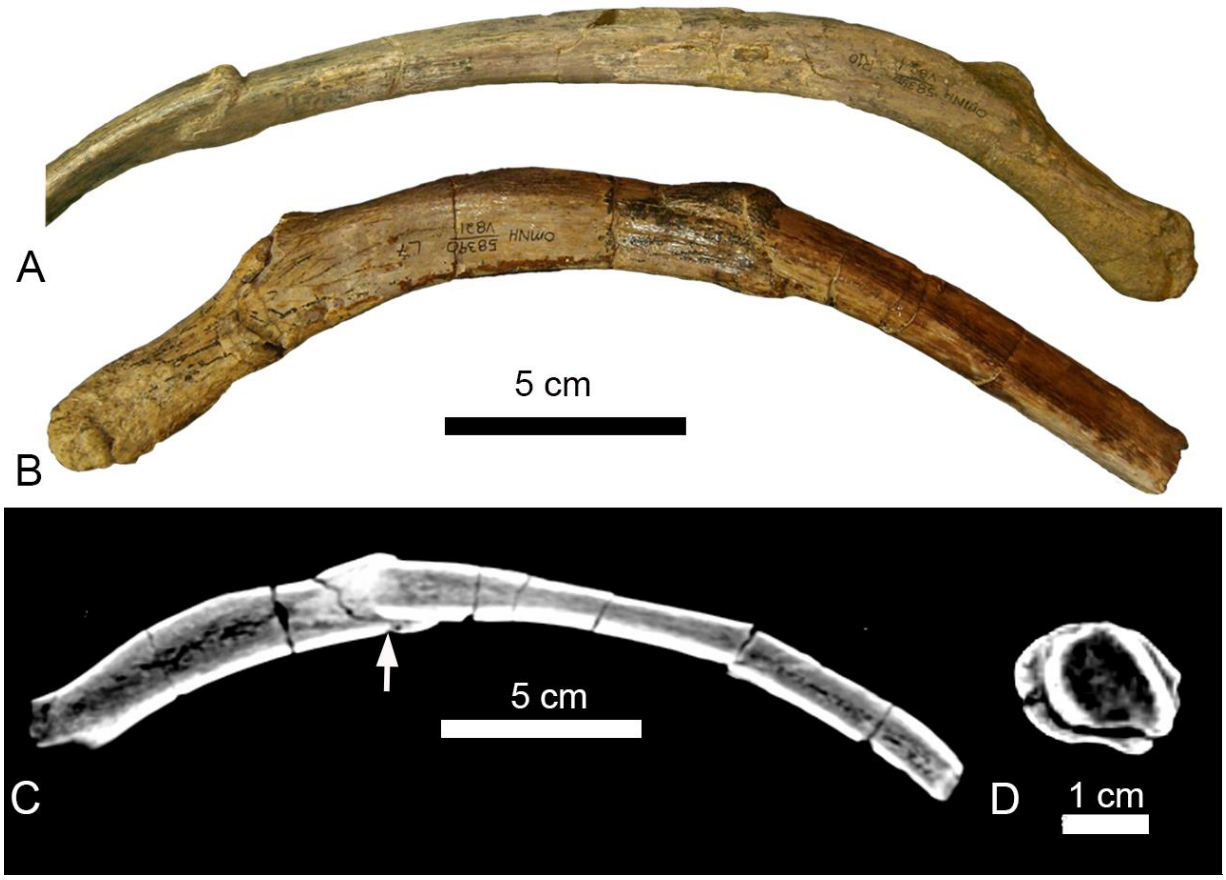

Figure 2: Fractured right dorsal rib (R10) (A.) and fractured left dorsal rib (L7) (**B**–**D)**. **A.** R10 in anterior view **B.** L7 in anterior view **C.** Anterior slice through L7 showing 24 mm of compaction and angulation of the distal rib element. **D.** Cross-section of rib L7 in proximal view, location of slice indicated by the white arrow in **C**. The slice shows the stacked cortical bone resulting from the impaction of the distal rib element into the proximal element. The lack of callus formation indicates this fracture is perimortem. The pathology is classified as traumatic.

Figure 3: **A.** Left dorsal rib 10 (L10) in anterior view showing a callus that has expanded the shaft of the rib. **B.** Enlarged anterior view of callus surface showing eye-shaped callus margin with two lytic lesions present on the callus margin. These lesions are suggestive of osteomyelitis (a traumatic-infectious pathology).

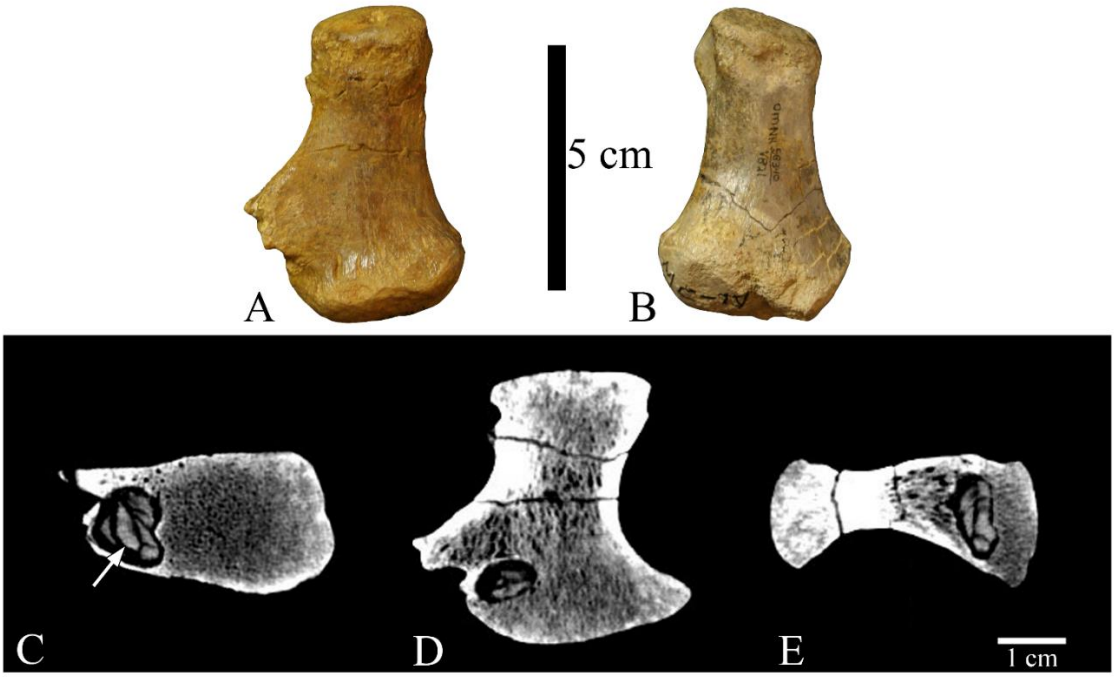

Figure 4: OMNH 58340 left and right metacarpal IV. **A**. Left metacarpal IV dorsal view **B.** Right metacarpal IV dorsal view. **C-E.** Computed tomography scans of left metacarpal IV showing the internal morphology consistent with a type of subacute pyogenic osteomyelitis called a Brodie abscess. **C.** Proximal view **D.** Dorsal view **E.** Lateral view. Arrow indicates the presence of an irregular sequestrum within the abscess consistent with a Brodie abscess in an early stage of its development.